Hindawi Publishing Corporation
Applied Bionics and Biomechanics
Volume 2016, Article ID 1712831, 10 pages
http://dx.doi.org/10.1155/2016/1712831

Research Article

Design of a Reconfigurable Robotic System for Flexoextension Fitted to Hand Fingers Size

J. Felipe Aguilar-Pereyra[1,2] and Eduardo Castillo-Castaneda[1]

[1]*Centro de Investigación en Ciencia Aplicada y Tecnología Avanzada, Instituto Politécnico Nacional, 76090 Querétaro, QRO, Mexico*
[2]*División de Tecnologías de Automatización e Información, Universidad Tecnológica de Querétaro, Querétaro, QRO, Mexico*

Correspondence should be addressed to J. Felipe Aguilar-Pereyra; faguilar@uteq.edu.mx

Received 15 January 2016; Revised 12 April 2016; Accepted 19 May 2016

Academic Editor: Jie Liu

Due to the growing demand for assistance in rehabilitation therapies for hand movements, a robotic system is proposed to mobilize the hand fingers in flexion and extension exercises. The robotic system is composed by four, type slider-crank, mechanisms that have the ability to fit the user fingers length from the index to the little finger, through the adjustment of only one link for each mechanism. The trajectory developed by each mechanism corresponds to the natural flexoextension path of each finger. The amplitude of the rotations for metacarpophalangeal joint (MCP) and proximal interphalangeal joint (PIP) varies from 0 to 90° and the distal interphalangeal joint (DIP) varies from 0 to 60°; the joint rotations are coordinated naturally. The four R-RRT mechanisms orientation allows a 15° abduction movement for index, ring, and little fingers. The kinematic analysis of this mechanism was developed in order to assure that the displacement speed and smooth acceleration into the desired range of motion and the simulation results are presented. The reconfiguration of mechanisms covers about 95% of hand sizes of a group of Mexican adult population. Maximum trajectory tracking error is less than 3% in full range of movement and it can be compensated by the additional rotation of finger joints without injury to the user.

1. Introduction

The number of people with disabilities is increasing; thus, the demand of rehabilitation services is increasing too, due to the population growth and ageing, emerging chronic diseases, and the medical advances that preserve and extend life expectancy [1]. The World Health Organization reported "an estimated 10% of the world's population, some 650 million people, experience some form of impairment or disability"; about 80% of people with disabilities live in developing countries. The majority are poor and experience difficulties in accessing basic health services, including rehabilitation services [1], an alternative to address this problem is the use of robotic systems in rehabilitation therapies. Robotic systems have already proven to enhance hand therapies through incorporating intensive and interactive exercises [2, 3]. Levanon confirms that "advanced technology can enrich treatment and can help patients who cannot come to the clinic regularly for treatment" [4]. "Disorders of the upper extremities specifically limit the independence of affected subjects" [5] and impairment of hand affects significantly the execution of activities of daily living (ADL). There are injuries like fractures, sprains, and dislocations that cause temporary disability and they require mobilization exercises as part of rehabilitation therapy [6]. Fasoli et al. concludes that "robotic therapy may complement other treatment approaches by reducing motor impairment in persons with moderate to severe chronic impairments" [7]. On the other hand, Carey et al. concluded "that individuals with chronic stroke receiving intensive tracking training showed improved tracking accuracy and grasp and release function, and these improvements were accompanied by brain reorganization" [8]. Thus, Kitago et al. stablish that there is a great need to develop new approaches to rehabilitation of the upper limb after stroke. Robotic therapy is a promising form of neurorehabilitation that can be delivered in higher doses than conventional therapy [9]. Additionally, rehabilitation robots also can be a platform for quantitative monitoring on

the recovery process in a rehabilitation program due to the standardized experimental setup and the high repeatability of motion tasks.

Different robotic devices for upper limb rehabilitation have been developed over the past two decades to provide hand motor therapy [5]. There are different design philosophies applied to robotic therapies, determining the degrees of freedom considered and technologies used. The objective is to develop a training platform that helps patients regain hand range of motion and the ability to grasp objects, ultimately allowing the impaired hand to partake in activities of daily living [10].

In the specific case of the fingers of the hand, exoskeletons, wearable orthosis and gloves, haptic interfaces, and end-effector-based devices have been developed and evaluated in order to facilitate the rehabilitation process [3, 5]. Exoskeletons are devices with a mechanical structure that mirrors the skeletal structure of the limb; that is, each segment of the limb associated with a joint movement is attached to the corresponding segment of the device. This design allows independent, concurrent, and precise control of movements in a few limb joints. It is, however, more complex than an end-effector-based device [5]. An example of this approach is the HEXORR, Hand EXOskeleton Rehabilitation Robot [10]. This device has been designed to provide full range of motion (ROM) for all of the hand's digits. The thumb actuator allows for variable thumb plane of motion to incorporate different degrees of extension-flexion and abduction-adduction. The finger four-bar linkage is driven by a direct current, brushless motor. The mechanisms of HEXORR only have one rotation axis for all the metacarpophalangeal joints for index to little fingers, but the rotation axes of the finger joints are not collinear. This device does not consider the distal interphalangeal joins of the fingers.

Glove devices are wearable, such as the robotic glove, which utilizes soft actuators consisting of molded elastomeric chambers with fiber reinforcements that induce specific bending, twisting, and extending trajectories under fluid pressurization. These soft actuators were mechanically programmed to match and support the range of motion of individual fingers [11]. These devices require a pneumatic or hydraulic facility, which is more complex than electric supply, especially for domestic use. The variation in hand size can be a complication for the use of these devices.

The haptic devices form another group of systems interacting with the user through the sense of touch and the mobilization of the limb. Haptic devices can be classified as either active or passive, depending on their type of actuator. An example of this approach is the "haptic knob" which is a two-degree-of-freedom robotic interface to train movements and force control of wrist and hand. The "haptic knob" uses an actuated parallelogram structure that presents two movable surfaces that are squeezed by the subject [12]. This device is oriented to perform many ADL such as grasping and manipulating objects.

The advantage of the end-effector-based systems is their simpler structure and thus less complicated control algorithms. However, it is difficult to isolate specific movements of a particular joint. The Rutgers Hand Master II is a force-feedback glove powered by pneumatic pistons positioned in the palm of the hand and provides force feedback to the thumb, index, middle, and ring fingertips [13]. The fingertips develop a linear trajectory, whose amplitude depends on the length of the pneumatic pistons. Amadeo is a commercially available device that provides endpoint control of each of the hand digits along linear fixed trajectories electric motor [14]. In this case, the fingertips develop a linear trajectory too.

The design of a reconfigurable robotic system proposed, Ro-Share, has advantages with respect to the devices mentioned. First, it is designed so that each fingertip develops a natural flexoextension trajectory considering the joint coordination of each finger kinematic chain. Each of the fingers is free to move without forcing the rotation axis alignment of its joints. Only one actuator is necessary for each mechanism that mobilizes one finger. Each mechanism can be adjusted to the finger length by the length adjustment of its crank link. The variation of hand length can be up to 16% for a male and female adult from 18 to 90 years old specific population [15]. Hence, a robotic system to guide the fingertip of fingers, index, middle, ring, and little finger, in flexion and extension exercises is proposed, which must be able to fit finger sizes through only one link length adjustment.

2. Methods

2.1. Kinematic Hand Model. The general structure of the human hand can be divided into two sets for its kinematic analysis. The first set is composed of the bones of carpus and the second of the metacarpals link and the phalanges of the five digits [16, 17]. A realistic approach, useful for flexoextension exercises of the fingers in rehabilitation therapies, considers for the fingers from the index to the little finger a kinematic chain with 3 links, which are the phalanges, and 4 degrees of freedom (DOF). For the thumb, the kinematic chain has 3 links, the metacarpal (MC), 2 phalanges, and 5 DOF. The palm of the hand is considered a fixed base. In this approach, for the index finger to the little finger, the metacarpals (MC) represent the immobile base of each kinematic chain. This is complemented by the proximal phalange (PP), medial phalange (MP), and distal phalange (DP) as links, as shown in Figure 1. The metacarpophalangeal joint (MCP) has 2 DOF, and the interphalangeal joints, proximal (PIP) and distal (DIP), have only one DOF. P represents the fingertip, the mobile end of the kinematic chain. The joins of the thumb are the carpometacarpal (TCMC) with 2 DOF, the metacarpophalangeal (TMCP) with 2 DOF, and the proximal interphalangeal joint (PIP) with one DOF.

The Denavit-Hartenberg (D-H) convention is used to define each one of the four kinematic chains [18, 19]. Table 1 presents the D-H parameters of kinematic chains, where LPP, LMP, and LDP are the nominal lengths of the proximal, medial, and distal phalanges, respectively.

Equation (1) describes the position and orientation of the fingertip [11]:

$$\begin{aligned} \mathrm{P}k = {}_{-1}^{0}T\left(u_k\right){}_{4}^{0}T\left(\theta_i\right)k = {}_{0}^{-1}T\left(u_k\right){}_{1}^{0}T\left(\theta_{\mathrm{MCPabd}}\right) \\ \cdot\, k\,{}_{2}^{1}T\left(\theta_{\mathrm{MCPflex}}\right)k\,{}_{3}^{2}T\left(\theta_{\mathrm{PIPflex}}\right)k\,{}_{4}^{3}T\left(\theta_{\mathrm{DIPflex}}\right)k, \end{aligned} \tag{1}$$

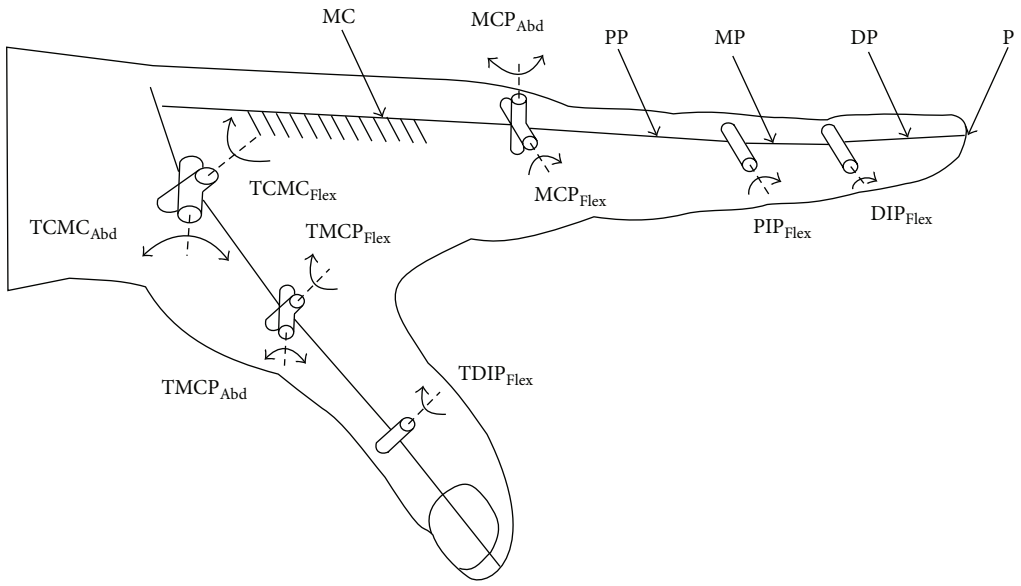

Figure 1: Kinematic model of hand with fixed metacarpal (except thumb).

Table 1: D-H parameters of kinematic chains corresponding to the index to little fingers, considering metacarpal links fixed.

Joint	θ_i	d_i	a_i	α_i
1	$\theta_{\text{MCP abd}}$	0	0	$\pi/2$
2	$\theta_{\text{MCP flex}}$	0	LPP	0
3	$\theta_{\text{PIP flex}}$	0	LMP	0
4	$\theta_{\text{DIP flex}}$	0	LDP	0

Table 2: Angles of active movements of the joints of the fingers: index to little finger.

Finger\joint	$\theta_{\text{MCP abd}}$	$\theta_{\text{MCP flex}}$	$\theta_{\text{PIP flex}}$	$\theta_{\text{DIP flex}}$
Index	20–30°	90°	110°	80°–90°
Middle	20–30°	90°	110°	80°–90°
Ring	20–30°	90°	120°	80°–90°
Little	20–30°	90°	135°	90°

where Pk represents an array containing the position and orientation of the fingertip, and k is the indicator for the fingers: index = 2, medium = 3, ring = 4, and little finger = 5, since 1 is reserved for the thumb. $T(u_k)$ represents the vector used to define the reference frame at the origin of the kinematic chain of each finger relative to a fixed frame of reference at the base of the hand. $T(\theta_i)k$ are the homogeneous transformation matrices which define the geometric transformation between the origin of the kinematic chain of each finger and its tip. According to [16, 17], rotation of the finger joints is shown in Table 2. Figure 2 shows the path of flexoextension of the kinematic chain of the three phalanges of the middle finger. This path fingertip (P) is the initial requirement for movement of the flexoextensor mechanisms of the robotic system.

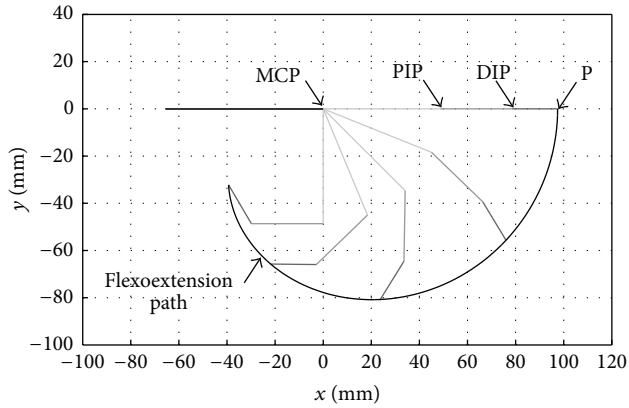

Figure 2: Flexoextension path of the kinematic chain of the three phalanges of middle finger (0° ≤ MCP ≤ 90°, 0° ≤ PIP ≤ 90°, and 0° ≤ DIP ≤ 60°).

2.2. Proposed R-RRT Mechanism. The characteristics of simplicity, modularity, and low cost of construction and maintenance are desirable in devices for assistance in rehabilitation therapies [20]. The most important criterion is the patient's safety; therefore, the range of movement of flexoextensor mechanism R-RRT is mechanically limited to avoid finger hyperextension. Accuracy in the tracking of the flexoextension path is the second aspect of importance, since continuous and gentle movements are desired from the beginning (Lim_{ext}) to the end of the path (Lim_{flex}). Therefore, the position and velocity of movements should be controlled. Exercises can start with movements of low amplitude and low speed and increase both amplitude and speed up to the full range of flexion and extension. Therapies must be always supervised by professional physiotherapists to avoid sudden movements that can cause pain or further damage to the

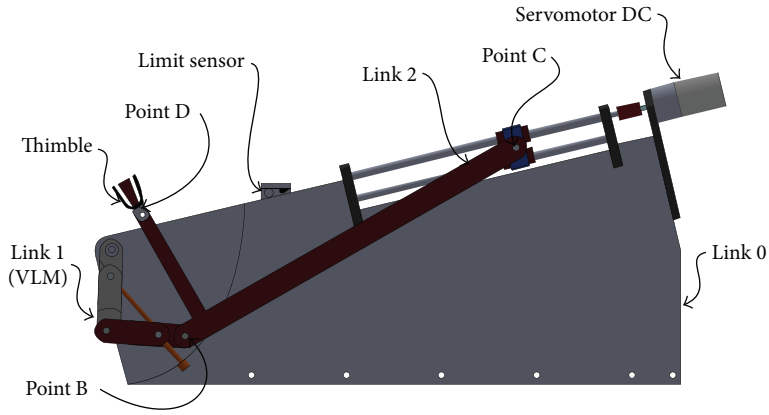

Figure 3: R-RRT mechanism of the middle finger.

patient. In response to the above requirements, the system is composed of four four-bar type crank-slide mechanisms (R-RRT) for the mobilization of the fingers from the index to the little finger.

Figure 3 shows the corresponding mechanism design for middle finger. The DC servomotor drives point C of the slide on a linear guide through the screw, foregoing causes semicircular movements of point B of the variable length crank (VLC). Finally, point D of the coupler link develops the flexoextension path. Point D is attached to the fingertip P through a thimble secured by adhesive tape for medical use. The thimble has an unactuated joint to connect itself with link 2 (coupler) at point D; it allows the free rotation of the thimble and the natural orientation of the distal phalange. As an additional safety, a limit sensor detects when the mechanism reaches the positions of maximum flexion or extension, to indicate to an electronic controller these positions. The R-RRT, type slider-crank mechanism, is selected since the extension of the coupler link develops a very similar path presented in Figure 2. Each flexoextensor mechanism (R-RRT) develops the flexoextension path in the distal end of the extension of the coupler link (D), Figure 4(a).

The length of each finger defines the dimensions of the corresponding mechanism. The synthesis of flexoextensor mechanisms was performed from a trajectory generation method using 3 precision points based on the curves of the coupler link [21].

A major constraint is that the length of the extension of the coupling link, L_3, must be greater than the length of the crank, L_2, to avoid collisions between finger and mechanism. The lengths of link 2, L_2, and the extension of the coupler link, L_3, are defined by (2) and (3), respectively,

$$L_2 = L_1 * 6.21, \tag{2}$$

$$L_3 = L_1 * 1.2. \tag{3}$$

Due to the length of the crank handle that determines the range of movement on the x-axis, the path of flexoextension, Figure 2, was rotated the angle α, Figure 5(a); after this, the rotated path was moved to point $(0, 0)$ using a homogeneous transformation matrix H. Finally, the start and the end of the path are aligned with the axis x and the position of the maximum flexion meets with point $(0, 0)$, Figure 5(b).

The rotation angle is calculated with

$$\alpha = \tan^{-1}\left(\frac{y_{\text{Fmax}} - y_{\text{Emax}}}{x_{\text{Fmax}} - x_{\text{Emax}}}\right), \tag{4}$$

where x_{Fmax}, y_{Fmax}, x_{Emax}, and y_{Emax} are the coordinates of the maximum flexion position (Lim_{flex}) and maximum extension position (Lim_{ext}) of the natural flexoextension path in the axis x and y. Finally, the length of the crank link is calculated with

$$L_1 = \frac{\left(x_{\text{EmaxRot}} - x_{\text{FmaxRot}}\right)}{2}, \tag{5}$$

where x_{FmaxRot} and x_{EmaxRot} are the coordinates on the axis x of the positions of maximum extension and maximum flexion of the natural flexoextension path rotated on the angle α.

Once the mechanism has been synthesized, the orientation of the path is recovered by a rotation of the mechanism with the angle $-\alpha$ (equal magnitude than α but with opposite direction). Afterwards, an iterative numerical method to minimize the error path was later used [22].

2.3. Reconfiguration of R-RRT Mechanism. Each patient may have a different hand size, thus requiring the reconfiguration mechanism ability to adapt to flexoextension path. Therefore, a reconfiguration scheme to modify the path of point D of the coupler link is proposed in order to follow the path of flexoextension of the fingers for different sizes. For a group of Mexican population, the average hand size for adults between the ages of 18 and 90 is estimated at $\mu = 175.62$ mm with a standard deviation of $\sigma = 8,615$ mm [15]. If we consider a normal probability distribution, then, in the interval $[\mu - 2\sigma, \mu + 2\sigma]$, approximately 95% of the hand sizes for the Mexican population are understood. Therefore, it is estimated that hand size varies from 158.39 to 192.85 mm. The length of the crank link is half of straight length of the flexoextension rotated path on the x-axis. Then, changes in the length of the crank link can modify the path amplitude of point D of the mechanism. The design of a variable length crank link (VLC)

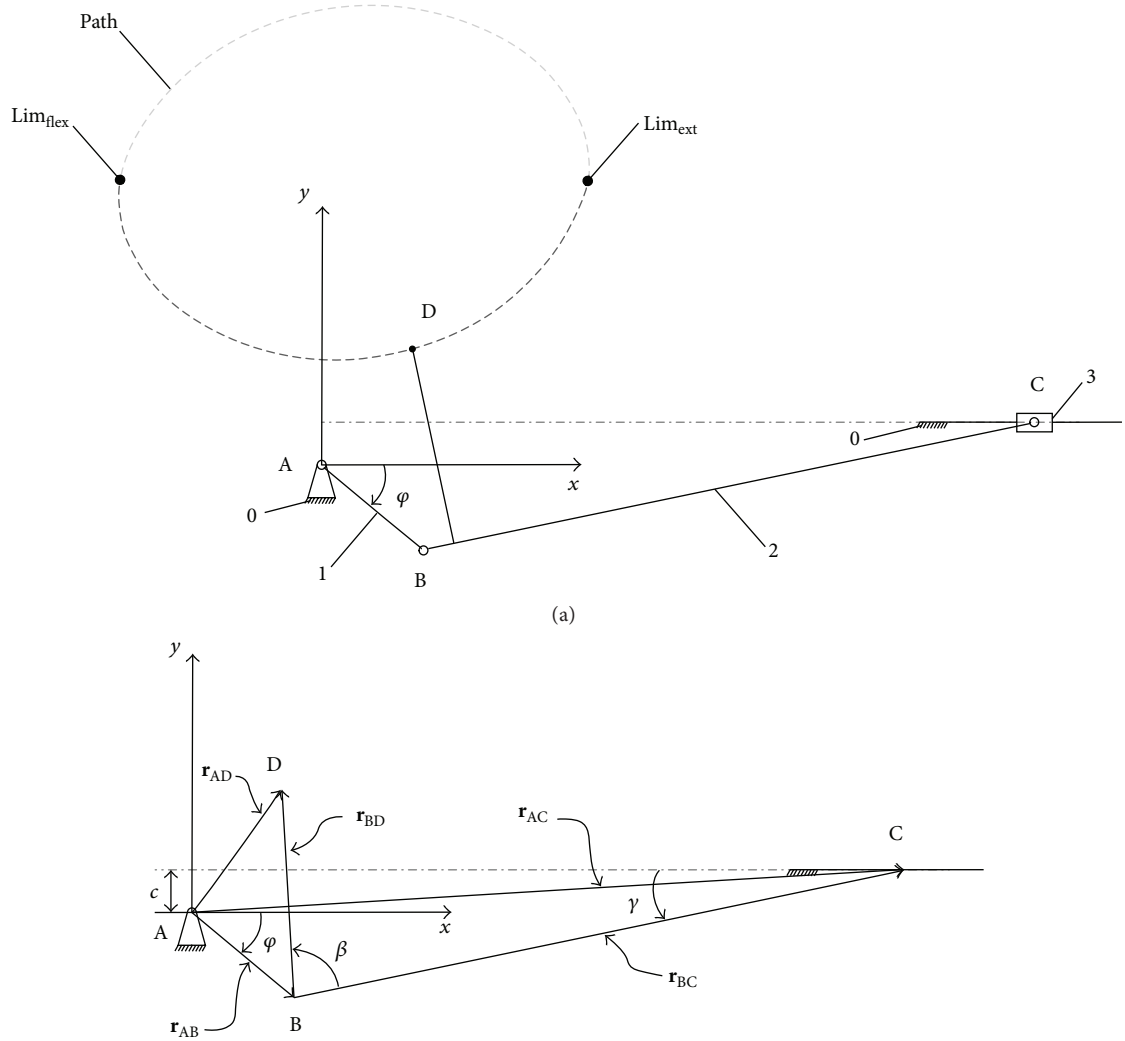

Figure 4: R-RRT mechanism: (a) scheme and (b) vector analysis.

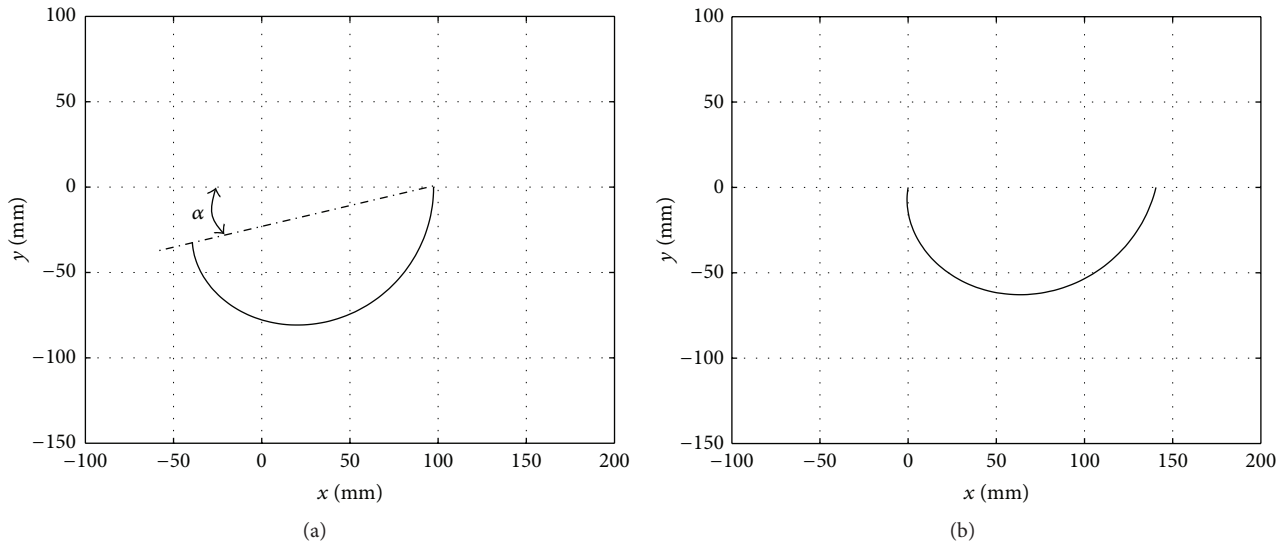

Figure 5: Flexoextension path: (a) rotation angle α and (b) rotated path.

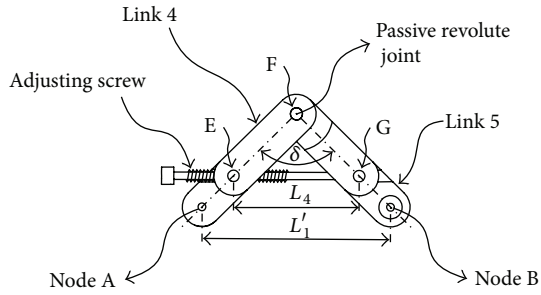

Figure 6: The variable length crank link (VLC).

is proposed in Figure 6, whose length L_1' between its external nodes A and B varies in proportion of length L_4. The VLC is composed of two links connected by a passive rotational joint, point F, and a screw whose end is attached to G point of link 5 through a ball joint, allowing only for rotation. The other point of contact between the screw and link 4 is achieved through a nut; so that when screw turns, L_4 varies. Similar triangles formed by points EFG and AFB, Figure 6, have the angle δ, *which is* defined by the law of cosines as

$$\delta = \cos^{-1}\left(\frac{L_4^2 + L_5^2 + L_6^2}{2 \cdot L_5 \cdot L_6}\right), \tag{6}$$

wherein L_5 and L_6 are the lengths of EF and FG lines, respectively, having the same length, $L_5 = L_6$.

The length L_1' is defined by

$$L_1' = \sqrt{(L_7^2 + L_8^2 - 2 \cdot L_7 \cdot L_8 \cdot \cos\delta)}, \tag{7}$$

wherein L_7 and L_8 are the lengths of AF and FB respectively, which have the same length, $L_7 = L_8$.

2.4. Kinematic Analysis of R-RRT Mechanism. In order to validate the monitoring path of flexoextension of the proposed mechanism, kinematic analysis of the synthesized mechanism is performed and the tracking error of the path is calculated. Vector loop method is used for position analysis [21]. A right-handed coordinate system is defined and a local reference frame x, y is located at point A of fixed link 0. Each mechanism has a point A, which is the point of rotation of the crank, link 1. Point B is in the joint that connects the crank link to the coupler, link 2; point B develops a circular constant radius equal to the crank's length. Point C, corresponding to the slide, moves on a linear axis parallel to the x-axis. Finally, point D, located in the extension of the coupler link, develops an elliptical path that, in the range of $180^\circ \leq \theta \leq 360^\circ$, is similar to the flexoextension path, Figure 2.

Vectors $\mathbf{r}_{AB}$ and $\mathbf{r}_{BC}$ correspond to links 1 and 2, respectively, Figure 4(b), so that their magnitudes are constant. Point C is defined by the $\mathbf{r}_{AC}$ vector, whose magnitude varies according to angle φ, since it is the sum of vector $\mathbf{r}_{AB}$ and $\mathbf{r}_{BC}$. The $\mathbf{r}_{AC}$ vector has the following components: x_{AC} that is parallel to the sliding axis of the slide and y_{AC} which is constant and corresponds to the length of offset (c) between the axis of the extended slide shaft and pivot of the link [21]. The most important point is D, because it performs the desired path and is defined by $\mathbf{r}_{AD}$ vector, which is the result of the sum of $\mathbf{r}_{AB}$ and $\mathbf{r}_{BD}$ vectors (8). The magnitude of $\mathbf{r}_{BD}$ vector is constant, since it corresponds to the extension length of the coupler link; angle β is a constant value that determines the orientation according to $\mathbf{r}_{BC}$ vector.

Position equation (8), velocity equation (9), and acceleration equation (10) of point D are calculated from the expressions:

$$\begin{aligned}\mathbf{r}_{AD} &= \mathbf{r}_{AB} + \mathbf{r}_{BD} = \left(x_{AB} + x_{BD}\right)\hat{\mathbf{i}} + \left(y_{AB} + y_{BD}\right)\hat{\mathbf{j}} \\ &= \left(L_1\cos\varphi + L_3\cos\psi\right)\hat{\mathbf{i}} + \left(L_1\sin\varphi + L_3\sin\psi\right)\hat{\mathbf{j}},\end{aligned} \tag{8}$$

$$\begin{aligned}\mathbf{v}_{AD} &= \dot{\mathbf{r}}_{AD} = \dot{\mathbf{r}}_{AB} + \dot{\mathbf{r}}_{BD} = \left(\dot{x}_{AB} + \dot{x}_{BD}\right)\hat{\mathbf{i}} + \left(\dot{y}_{AB}\right. \\ &\left. + \dot{y}_{BD}\right)\hat{\mathbf{j}} = -\left(L_1\dot{\varphi}\sin\varphi + L_3\dot{\psi}\sin\psi\right)\hat{\mathbf{i}} \\ &+ \left(L_1\dot{\varphi}\cos\varphi + L_3\dot{\psi}\cos\psi\right)\hat{\mathbf{j}},\end{aligned} \tag{9}$$

$$\begin{aligned}\mathbf{a}_{AD} &= \ddot{\mathbf{r}}_{AD} = \ddot{\mathbf{r}}_{AB} + \ddot{\mathbf{r}}_{BD} = \left(\ddot{x}_{AB} + \ddot{x}_{BD}\right)\hat{\mathbf{i}} + \left(\ddot{y}_{AB}\right. \\ &\left. + \ddot{y}_{BD}\right)\hat{\mathbf{j}} = \left(-L_1\ddot{\varphi}\sin\varphi - L_1\dot{\varphi}^2\cos\varphi - L_3\ddot{\psi}\sin\psi\right. \\ &\left. - L_3\dot{\psi}^2\cos\psi\right)\hat{\mathbf{i}} + \left(L_1\ddot{\varphi}\cos\varphi - L_1\dot{\varphi}^2\sin\varphi\right. \\ &\left. + L_3\ddot{\psi}\cos\psi - L_3\dot{\psi}^2\sin\psi\right)\hat{\mathbf{j}},\end{aligned} \tag{10}$$

where L_1 is the length of segment AB, L_3 is the length of segment BD, and $\dot{\varphi}$ and $\ddot{\varphi}$ are the angular velocity and acceleration, respectively.

3. Results

3.1. Construction Parameters. The reconfigurable robotic system for flexoextension is composed of four four-bar mechanisms and it is complemented with a variable height base on which the forearm and palm rest, Figure 7. Table 3 shows parameters of construction of four mechanisms corresponding to the index, middle, ring, and little fingers.

Figure 8 shows the behavior of the position, velocity, and acceleration of point D of the mechanism of the middle finger in the x- and y-axes. It is observed that all the curves are smooth and continuous in the range of the path from the maximum extension (Lim_{ext}) up to the maximum finger bending (Lim_{flex}).

Figure 9 illustrates the final work area of the flexoextensor reconfigurable mechanism for the case of the middle finger. The central path corresponds to the average hand size (175.62 mm) and external paths correspond to the minimum (158.39 mm) and maximum (192.85 mm) size of the Mexican adults between 18 and 90 [8]. The area between the latest two paths corresponds to the area of work expanded by reconfiguring the variable length crank link (VLC). However, after adjusting the length of the handle, it will not move until required by another patient.

3.2. Path Tracking Error. In order to determine the tracking error according to the natural course of the flexoextension path of the middle finger, the difference between the OD and OP vectors is measured. The maximum error has a value of

Table 3: Construction parameters for the four R-RRT mechanisms.

Finger/length	L_1 min (mm)	L_1 max (mm)	L_2 (mm)	L_3 (mm)	L_5 (mm)	L_7 (mm)	β (°)
Index	47.15	77.70	387.66	74.90	26.67	44.46	80
Middle	53.08	87.48	436.44	84.33	30.03	50.05	80
Ring	50.01	82.42	411.19	79.45	28.29	47.15	80
Little	38.78	63.91	318.85	61.61	21.94	36.56	80

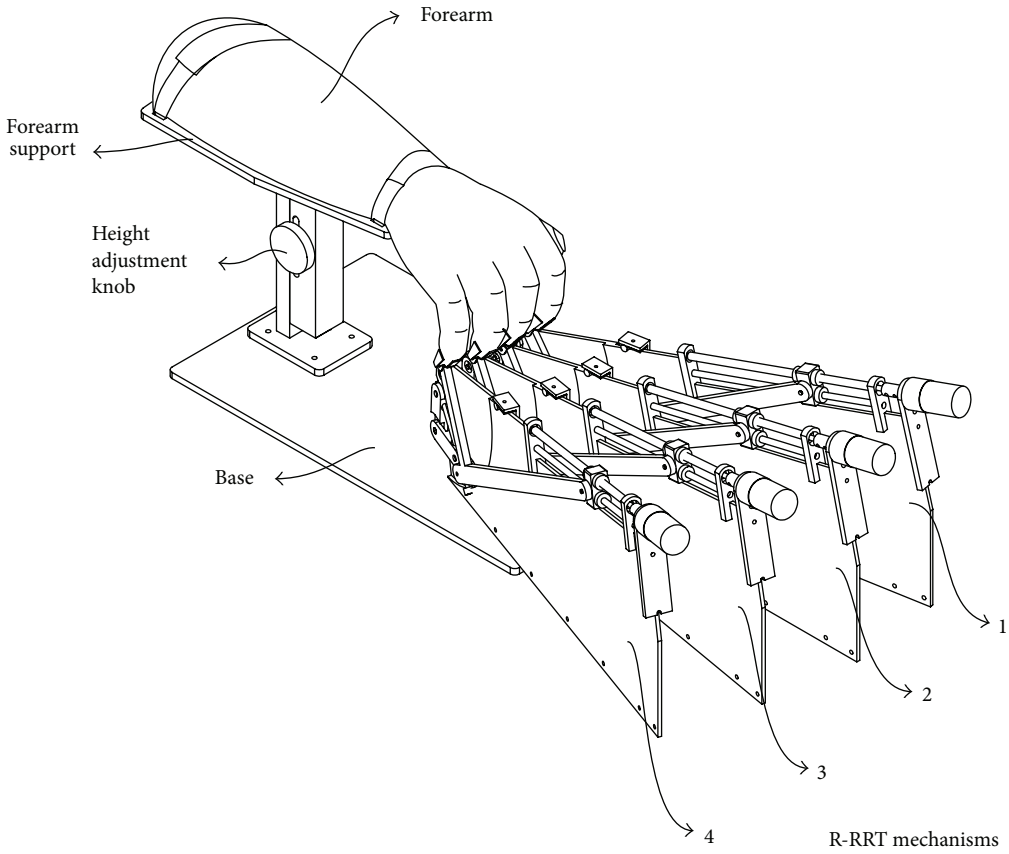

Figure 7: General view of the of the flexoextensor robotic system mechanisms.

2.98%. Figure 10 shows the graph of error in the range of movement of the crank link.

The patient hand size is bounded in the range of 158.39 mm to 186.63 mm and is divided into eight intervals with increments of 4.30 mm. With the constant value of the length of the coupler link L_2 = 436.44 mm, length of the extension of the coupler link L_{ext} = 84.33 mm, and the extension of the coupler link angle β = 80° = 1.396 radians, only the length of the link is modified and the paths are shown in Figure 11. Table 4 shows the values of nine hand sizes and their maximum tracking error obtained.

3.3. Abduction Movement. In natural extension movements of the hand fingers, an abduction movement is also developed by index, ring, and little finger. When the MCP joint is flexed, the lateral ligaments are tight; it makes the abduction movements difficult or impossible [16]. The index, ring, and little fingers have major amplitude of abduction movement as 30° [Cobos]. The position of each R-RRT mechanism has the maximum flexion point as reference; in this case, the middle finger does not develop the abduction; then, middle finger mechanism orientation is parallel with the arm longitudinal axis. The mechanism orientation for index, ring, and little fingers allows an abduction movement, which begins with 0° in maximum flexion and ends with an angle γ in maximum extension. If the angle γ takes the value of the half of maximum abduction; then, γ = 15°. The result is an abduction movement of 15° for index and ring finger with reference to middle finger, and 15° of little finger with reference to ring finger. This results in comfortable movements for four fingers, index to little finger, and the metacarpophalangeal joint movement in flexoextension and abduction.

4. Conclusions

The design of the reconfigurable robotic system for flexoextension can be adapted to the size of the hand; it is the result of a compromise between functionality and

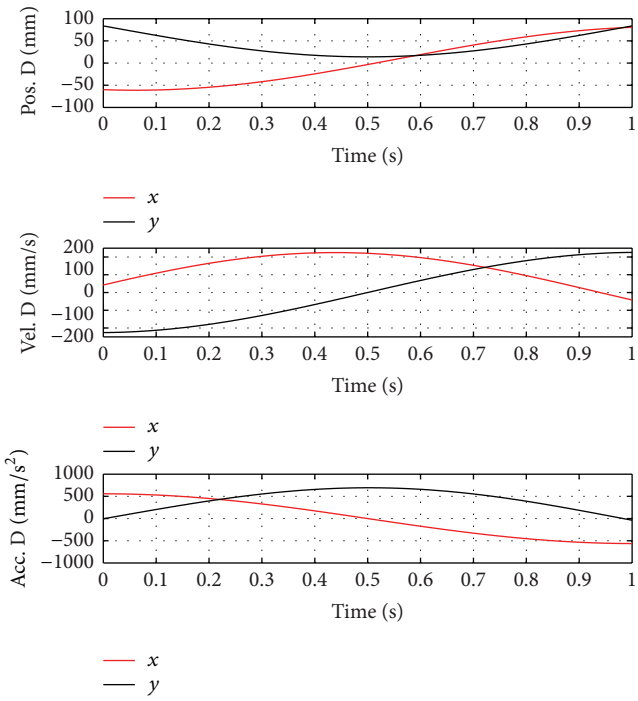

Figure 8: Result of position, velocity, and acceleration of point D, for $180^\circ \leq \varphi \leq 360^\circ$.

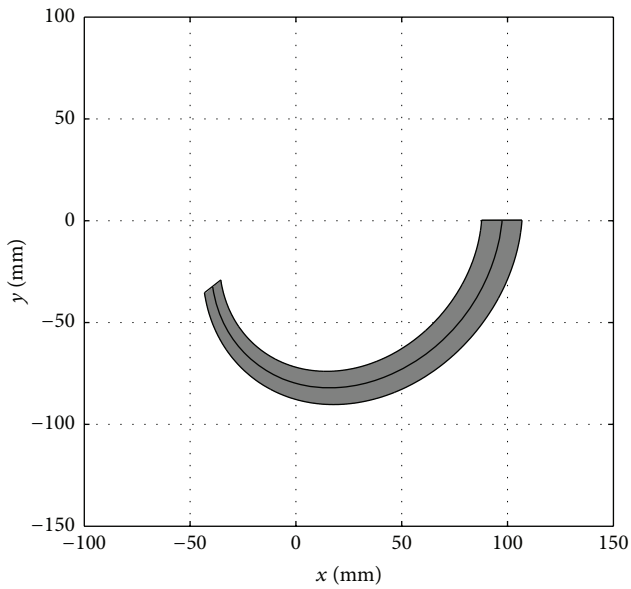

Figure 9: Work area of reconfigurable flexoextensor mechanism (the middle finger case).

practicality required for the movement of the fingers as part of rehabilitation therapies. The movement of the fingers is performed following their natural flexoextension path and prevents hyperextension, ensuring that the fingers never perform unnatural movements. The four R-RRT mechanisms orientation allows a 15° abduction movement for index, ring, and little fingers. The reconfigurability of each of the four R-RRT mechanisms allows the system to fit the hand size of each patient, allowing attention to a larger percentage of the population considered for design.

Table 4: Maximum tracking error for different lengths of hand.

Point	Hand size (mm)	Length of crank (mm)	Maximum tracking error (%)
1	158.39	53.07	2.97
2	162.70	57.38	2.97
3	167.01	61.68	2.97
4	171.31	65.98	2.97
5	175.62	70.28	2.97
6	179.93	74.56	2.96
7	184.24	78.88	2.96
8	188.54	83.18	2.96
9	192.85	87.48	2.97

An advantage of our proposal is related to the patient comfort; that is, the patient's hand should not carry anything, since it is based on the system. This represents an advantage over gloves or exoskeletons whose mass must be loaded by the user's hand. The system will provide the required forces to move the fingers and allow the physiotherapist, by means of an electronic control system, to monitor and record the progress for evaluation of both the evolution of patients and rehabilitation protocols. Levanon says that "... technology is the language of the next generation and therapists must adapt the types of treatments that are able to provide their customers, and they need to be enabled to use family and significant equipment with customers in the future" [4].

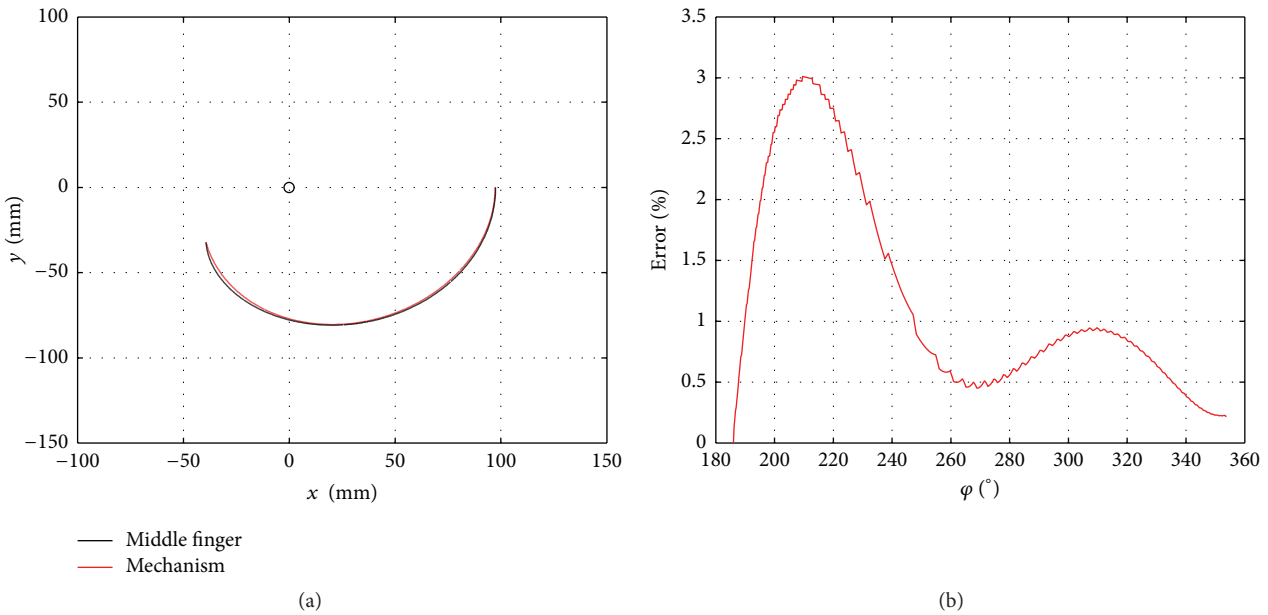

FIGURE 10: Error tracking of the mechanism (a) according to the natural path of flexion and extension of the middle finger and (b) percentage error in the path.

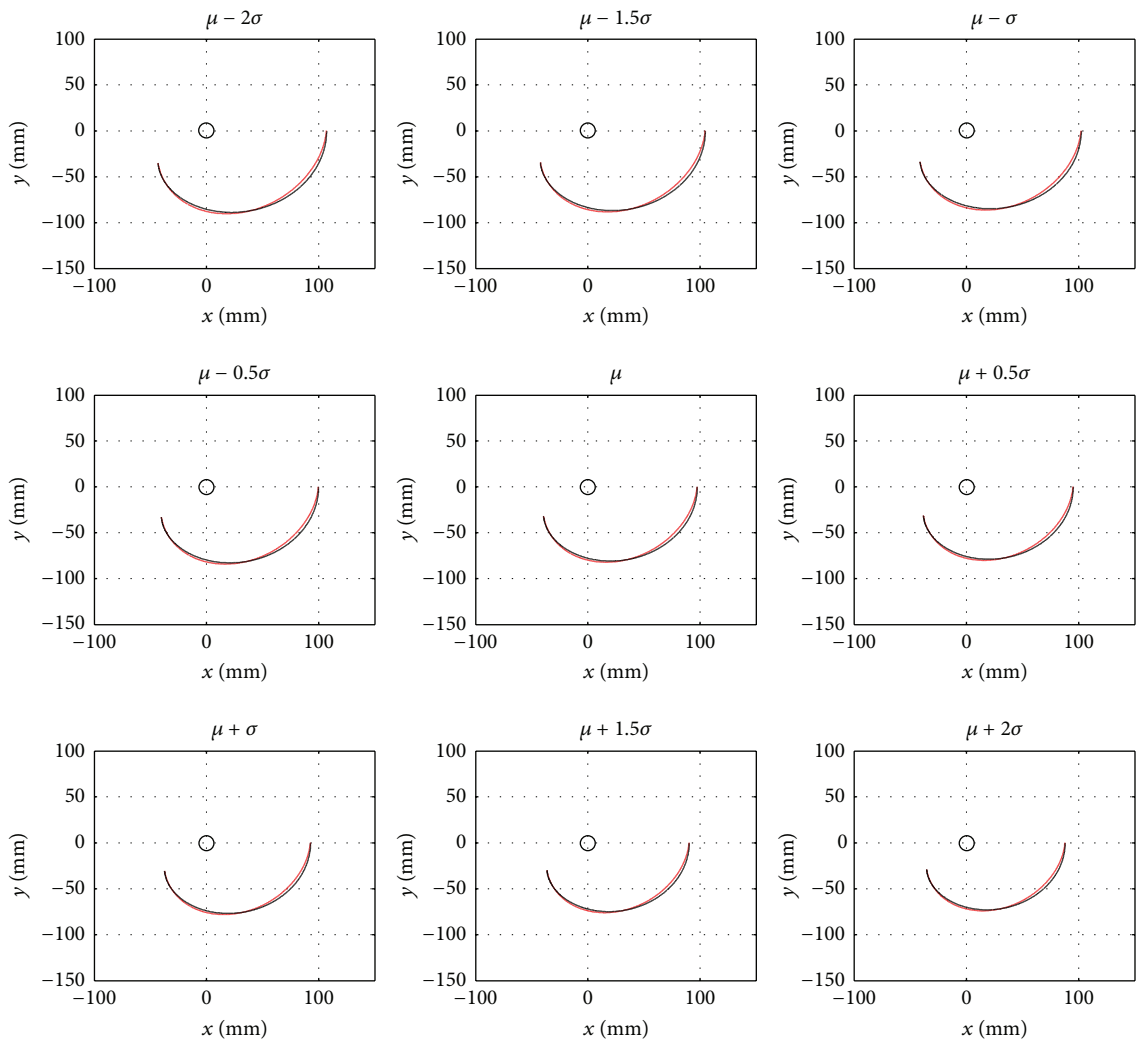

FIGURE 11: Paths of the middle finger and R-RRT proposed mechanism.

Competing Interests

The authors declare that they have no competing interests.

Acknowledgments

The authors would like to acknowledge the financial support of the institutions: Instituto Politécnico Nacional, Universidad Tecnológica de Querétaro and CONACYT, also CRIQ Centro de Rehabilitación Integral de Querétaro, and the therapists for their advice and discussion about rehabilitation protocols.

References

[1] WHO, *Disability and Rehabilitation*, World Health Organization, 2006, http://www.who.int/nmh/donorinfo/vip_promoting_access_healthcare_rehabilitation_update.pdf.pdf.

[2] C. G. Burgar, P. S. Lum, P. C. Shor, and H. F. Machiel Van der Loos, "Development of robots for rehabilitation therapy: the Palo Alto VA/Stanford experience," *Journal of Rehabilitation Research and Development*, vol. 37, no. 6, pp. 663–673, 2000.

[3] P. Heo, G. M. Gu, S.-J. Lee, K. Rhee, and J. Kim, "Current hand exoskeleton technologies for rehabilitation and assistive engineering," *International Journal of Precision Engineering and Manufacturing*, vol. 13, no. 5, pp. 807–824, 2012.

[4] Y. Levanon, "The advantages and disadvantages of using high technology in hand rehabilitation," *Journal of Hand Therapy*, vol. 26, no. 2, pp. 179–183, 2013.

[5] P. Maciejasz, J. Eschweiler, K. Gerlach-Hahn, A. Jansen-Troy, and S. Leonhardt, "A survey on robotic devices for upper limb rehabilitation," *Journal of Neuroengineering and Rehabilitation*, vol. 11, no. 1, article 3, 2014.

[6] A. Quesnot, J.-C. Chanussot, and R.-G. Danowski, "Main et doigts," in *Rééducation de l'Appareil Locomoteur. Tome 2 Membre Supérieur*, E. Masson, Ed., pp. 353–419, Elsevier Masson, 2nd edition, 2011.

[7] S. E. Fasoli, H. I. Krebs, J. Stein, W. R. Frontera, and N. Hogan, "Effects of robotic therapy on motor impairment and recovery in chronic stroke," *Archives of Physical Medicine and Rehabilitation*, vol. 84, no. 4, pp. 477–482, 2003.

[8] J. R. Carey, T. J. Kimberley, S. M. Lewis et al., "Analysis of fMRI and finger tracking training in subjects with chronic stroke," *Brain*, vol. 125, no. 4, pp. 773–788, 2002.

[9] T. Kitago, J. Goldsmith, M. Harran et al., "Robotic therapy for chronic stroke: general recovery of impairment or improved task-specific skill?" *Journal of Neurophysiology*, vol. 114, no. 3, pp. 1885–1894, 2015.

[10] C. N. Schabowsky, S. B. Godfrey, R. J. Holley, and P. S. Lum, "Development and pilot testing of HEXORR: hand EXOskeleton rehabilitation robot," *Journal of NeuroEngineering and Rehabilitation*, vol. 7, article 36, 2010.

[11] M. A. Delph, S. A. Fischer, P. W. Gauthier, C. H. M. Luna, E. A. Clancy, and G. S. Fischer, "A soft robotic exomusculature glove with integrated sEMG sensing for hand rehabilitation," in *Proceedings of the IEEE 13th International Conference on Rehabilitation Robotics (ICORR '13)*, June 2013.

[12] O. Lambercy, L. Dovat, V. Johnson et al., "Development of a robot-assisted rehabilitation therapy to train hand function for activities of daily living," in *Proceedings of the IEEE 10th International Conference on Rehabilitation Robotics (ICORR '07)*, pp. 678–682, Noordwijk, Netherlands, June 2007.

[13] M. Bouzit, G. Burdea, G. Popescu, and R. Boian, "The Rutgers Master II-new design force-feedback glove," *IEEE/ASME Transactions on Mechatronics*, vol. 7, no. 2, pp. 256–263, 2002.

[14] Tyromotion, AMADEO-Five Fingers. One Amadeo. For All Phases of Rehabilitation, 2016, http://tyromotion.com/en/products/amadeo.

[15] R. Ávila Chaurand, L. R. Prado León, and E. L. González Muñoz, *Demensiones antropométricas Población Latinoamericana*, Universidad de Guadalajara, Guadalajara, Mexico, 2nd edition, 2007.

[16] A. I. Kapandji, *Fisiología Articular: Esquemas Comentados de Mecánica Humana*, Editorial Médica Panamericana, Madrid, Spain, 6th edition, 2006.

[17] B. Tondu, "Kinematic modelling of anthropomorphic robot upper limb with human-like hands," in *Proceedings of the International Conference on Advanced Robotics (ICAR '09)*, pp. 1–9, IEEE, Munich, Germany, June 2009.

[18] J. Denavit and R. S. Hartenberg, "A kinematic notation for lower-pair mechanisms based on matrices," *Journal of Applied Mechanics*, vol. 23, pp. 215–221, 1955.

[19] J. J. Craig, *Introduction to Robotics: Mechanics and Control*, Addison-Wesley, Boston, Mass, USA, 2nd edition, 1955.

[20] C. E. Syrseloudis, I. Z. Emiris, T. Lilas, and A. Maglara, "Design of a simple and modular 2-DOF ankle physiotherapy device relying on a hybrid serial-parallel robotic architecture," *Applied Bionics and Biomechanics*, vol. 8, no. 1, pp. 101–114, 2011.

[21] R. L. Norton, *Design of Machinery: An Introduction to the Synthesis and Analysis of Mechanisms and Machines*, Mcgraw-Hill, New York, NY, USA, 5th edition, 2012.

[22] H. Zhou and K.-L. Ting, "Adjustable slider-crank linkages for multiple path generation," *Mechanism and Machine Theory*, vol. 37, no. 5, pp. 499–509, 2002.